Materials Advances

ROYAL SOCIETY OF CHEMISTRY

PAPER

View Article Online
View Journal | View Issue



Cite this: *Mater. Adv.*, 2025, **6**, 6152

# Spin-coated Ge–In–Se thin films: characterization and changes induced by visible and electron radiation in relation to indium content

Jiri Jancalek, [a] Aidan Milam, [b] Stanislav Slang, *[a] Michal Kurka, [a] Roman Svoboda, [c] Jiri Jemelka, [d] Miroslav Vlcek [ad] and Karel Palka [d]

Solution-processed $Ge_{25-x}In_xSe_{75}$ ($x$ = 0, 2.5, 5, 7.5 and 10) thin films were prepared *via* spin-coating for the first time. The glass transition temperature of source bulk glasses decreased with increasing indium content and subsequently guided the hard-baking temperatures of deposited thin films (60–240 °C). Energy-dispersive X-ray spectroscopy revealed thermally induced selenium loss at elevated temperatures, particularly in indium-rich compositions, and a greater resistance to organic residue removal with higher indium content. Increasing the hard-baking temperature led to structural changes resulting in decreased film thickness and optical bandgap, with a simultaneous increase in refractive index. At 240 °C, the optical parameters converged across indium-containing compositions, likely due to the content of low-index organics. Atomic force microscopy showed low surface roughness with minor porosity in $Ge_{17.5}In_{7.5}Se_{75}$, and $Ge_{15}In_{10}Se_{75}$ thin films. Raman spectroscopy confirmed thermal structural polymerization, with indium-based units showing difficult reintegration into the glass network. Photo- and electron-sensitivity studies using 532 nm laser exposure and electron beam lithography showed that 2.5 at% of indium significantly enhanced sensitivity, while further increases in indium content resulted in a gradual decline. Notably, $Ge_{22.5}In_{2.5}Se_{75}$ thin films exhibited an etching selectivity of 6.4, among the highest ever reported for solution-processed chalcogenide thin films.

Received 6th June 2025,
Accepted 27th July 2025

DOI: 10.1039/d5ma00596e

rsc.li/materials-advances



## Introduction

The chalcogenide glasses (ChGs) are amorphous semiconducting materials composed of chalcogen elements (S, Se or Te) combined with atoms typically from IV, V or VI group of the periodic table. ChGs possess a high refractive index, wide infrared transparency window, low phonon energy, and high ion conductivity.[1,2] Their unique properties can be harnessed in multiple forms, including bulk materials (*e.g.* lenses, windows, *etc.*),[3] fibers or amorphous thin films deposited on a suitable substrate (*e.g.* optical recording discs, diffractive optical elements, planar waveguides, high-resolution photoresists, *etc.*).[4–6] The ChG thin films are usually deposited from a gaseous phase using physical vapor deposition techniques (*e.g.* thermal evaporation, sputtering, laser ablation, *etc.*).[4,5,7,8] The vapor deposition techniques are well-established; however, they require expensive high vacuum instrumentation and present several challenges inherent to the specific nature of vacuum-based deposition method (*e.g.* composition fractionalization during thermal evaporation, limited size and lateral compositional gradient of sputtered and laser ablated thin films, *etc.*).[1,2,9]

Solution-processing deposition techniques (such as spin-coating, dip-coating, spiral bar-coating or electrospray)[10–16] offer a viable alternative to vacuum-based deposition methods. Solution processing is typically simpler, more cost-effective, and yields samples with good compositional homogeneity. The solution-processed thin films can also be embossed at lower temperatures than their vacuum-deposited counterparts,[17,18] resulting in reduced energy requirements. Additionally, novel composite materials can be easily produced as well, *e.g.* by dispersing nanoparticles in the glass solution.[19–21] ChGs are typically dissolved in volatile amine-based solvents and deposited thin films are treated by a combination of soft- and hard-baking to decompose formed chalcogenide salts, reduce the content of organic residuals, and polymerize the glass network. The organic residuals cannot be completely removed, and their remaining presence still limits certain applications of

[a] *Center of Materials and Nanotechnologies, Faculty of Chemical Technology, University of Pardubice, nam. Cs. legii 565, 53002 Pardubice, Czech Republic. E-mail: stanislav.slang@upce.cz*
[b] *Department of Chemistry, Austin Peay State University, 601 College St., Clarksville, TN, 37044, USA*
[c] *Department of Physical Chemistry, Faculty of Chemical Technology, University of Pardubice, Studentska 573, 53210 Pardubice, Czech Republic*
[d] *Department of General and Inorganic Chemistry, Faculty of Chemical Technology, University of Pardubice, Studentska 573, 53210 Pardubice, Czech Republic*

solution-processed thin films. However, they remain suitable for other photonic applications or spectral regions where absorption from organic residues is not critical. To date, solution-processing of chalcogenide glass thin films has not been implemented at the industrial level. In addition to challenges related to solvent residues, the range of suitable ChG compositions with diverse optical properties remains limited due to insufficient fundamental research.

The Ge–Se-based ChGs are good glass formers with covalently bonded network. Subsequently, the Ge–In–Se ternary system has a broad glass-forming range, extending up to 15 at% of indium.[22] The structure of Ge–In–Se glasses consists of 3D network of cross-linked $GeSe_2$ tetrahedral units and pyramidal units of $In_2Se_3$.[23,24] The indium introduction leads to notable changes in glass transition temperature $T_g$[25,26] along with an increase in electrical conductivity,[27] photoconductivity,[28] and optical nonlinearity.[29] These properties make Ge–In–Se ChGs suitable for photonic applications, fast optical switching devices and high-speed signal communication. Up to this day, the amorphous thin films of only several Ge-based chalcogenide systems were successfully deposited by solution processing from true (non-colloidal) glass solutions of amine-based solvents or their mixtures (Ge–S,[30] Ge–Se,[31] Ge–Sb–S,[32] and Ge–Sb–Se[33] systems with chalcogen overstochiometry). On the other hand, the crystalline $In_2Se_3$ thin films were prepared solely from highly toxic hydrazine[34] or amine-dithiol[35] solvents, whereas no solution-processed Ge–In–Se thin films have been yet deposited either in crystalline or amorphous form.[13,36]

In this study, we demonstrate the possibility for preparation of the $Ge_{25-x}In_xSe_{75}$ ($x$ = 0, 2.5, 5, 7.5 and 10) thin films from propylamine-methanol solvent mixtures. For the first time, the Ge–In–Se thin films were deposited *via* a solution route and in high optical quality. Differential scanning calorimetry (DSC) was used to determine the glass transition temperature ($T_g$) of the source bulk glasses, which in turn guided the selection of hard-baking temperatures for the solution-processed thin films. A combination of optical measurements, energy-dispersive X-ray spectroscopy (EDX) and Raman spectroscopy provided insight into the structural and compositional transformations occurring during the annealing of the as-prepared samples. The photo- and electron-sensitivity of hard-baked $Ge_{25-x}In_xSe_{75}$ thin films were investigated using a 532 nm laser beam exposure and electron beam lithography technique.

# Experimental methods

### Materials and chemicals

Germanium (Ge, 99.999%, Alfa Aesar), selenium (Se, 99.999%, Alfa Aesar), indium (In, 99.999%, Alfa Aesar), *n*-propylamine (PA, purum, ≥99.5%, Sigma Aldrich), ethylenediamine (EDA, ≥99.5%, Sigma Aldrich), methanol (MetOH, p.a., 99.5%, Lach-Ner), nitric acid ($HNO_3$, p.a., 65%, Lach-Ner), hydrochloric acid (HCl, p.a., 35%, Penta) and dimethyl sulfoxide (DMSO, p.a., Penta) were used without further purification. The PA, EDA, and MetOH were kept inside a nitrogen-filled glovebox (MBraun, MB200MOD; $O_2$, $H_2O$ content ≤ 0.1 ppm) due to the hygroscopicity of used solvents. Soda-lime substrates (Knittel Glass) were cleaned in aqua regia, rinsed with deionized water, and dried.

### Glass synthesis and thin film deposition

The $Ge_{25-x}In_xSe_{75}$ ($x$ = 0, 2.5, 5, 7.5 and 10) bulk glasses were prepared by the standard melt-quenching technique. High-purity 5N Ge, In and Se were loaded into pre-cleaned quartz ampules (cleaned with aqua regia and rinsed in deionized water) and sealed under a vacuum of $10^{-3}$ Pa. The glass synthesis was performed in a rocking tube furnace at 950 °C for 56 h. The quartz ampules with melted glass were subsequently rapidly quenched in cold water.

The synthesized bulk glasses were ground in an agate bowl, weighted into glass vials, and dissolved in a solvent mixture consisting of 10 vol% of MetOH in PA (PA-MetOH) with a concentration of 0.075 g of glass powder per 1 ml of solvent mixture. The dissolution was carried out inside a nitrogen-filled glovebox (MBraun, MB200MOD; $O_2$, $H_2O$ content ≤ 0.1 ppm) to prevent undesirable oxidation or hydrolysis. Glass vials were sealed and ChGs were dissolved under vigorous stirring at 400 rpm using a magnetic stirrer (Multistirrer Digital 6, Velp). Complete dissolution was achieved after 7 days, resulting in clear, homogeneous solutions without any visible precipitate or turbidity. Prior to thin film deposition, the solutions were filtered through a 220 nm PTFE filter to remove any potential microscopic aggregates.

The $Ge_{25-x}In_xSe_{75}$ thin films were deposited using a spin-coating technique (WS-650Mz-23NPPB, Laurell) inside the glovebox. A 150 μL of glass solution was dispensed onto rotating soda-lime glass substrates and spin-coated at 2000 rpm for 60 s. Freshly deposited thin films were immediately soft-baked at 60 °C for 20 min on a hot plate (HP 20D, Witeg) under an inert nitrogen atmosphere (hereafter referred to as "as-prepared" thin films). The as-prepared thin films were further thermally stabilized (hard baked) at 90, 120, 150, 180, 210, and 240 °C for 1 h, while the maximum annealing temperature was selected with respect to the $T_g$ of corresponding bulk glasses. The thermal stabilization process (hard baking) was again conducted inside a nitrogen-filled glovebox to prevent undesirable oxidation or hydrolysis.

### Characterization

The glass transition effect was recorded by differential scanning calorimetry technique using a heat flow DSC instrument (Q2000, TA Instruments, USA) equipped with an autosampler, RCS90 cooling accessory, and T-zero technology. The DSC was calibrated on the $H_2O$, In, and Zn standards. The samples of the chalcogenide glasses were measured in the form of single bulk pieces with approx. 10 mg mass (accurately weighted to 0.01 mg). The samples were inserted into the low-mass DSC pans and hermetically sealed, *i.e.* the measurements were performed in a static air atmosphere. The DSC measurements were realized as simple heating scans performed in the 50–450 °C temperature range at 10 °C $min^{-1}$. The characteristic glass transition temperature $T_g$ was evaluated from obtained

DSC curves (the $T_g$ values were determined, in accordance with the common practice, as half-height midpoints).

The surface morphology, cross-sections and elemental composition were analyzed by field emission scanning electron microscope (FE-SEM, LYRA 3, Tescan) equipped with an energy-dispersive X-ray (EDX) analyzer (AZtec X-Max 20, Oxford Instruments). The 20 nm carbon coating (Leica ACE200) was used to minimize the charging of prepared diffraction gratings. The SEM scans were recorded at 10 kV of acceleration voltage using a secondary electron detector. The EDX measurements were performed at 5 kV acceleration voltage on five distinct 400 × 400 μm areas. The EDX results were processed in AZtec software (Oxford Instruments), averaged and error bars represent the standard deviation from averaged values. The LYRA 3 microscope was also employed for electron beam lithography (EBL), with exposure doses ranging from 50 to 1250 μC cm$^{-2}$. The latent images of test dose patterns were subsequently developed *via* wet etching (details provided below).

The transmission spectra of prepared thin films were recorded by UV-VIS-NIR spectrometer (Shimadzu UV3600 Plus) in the spectral range 190–2000 nm. The thickness and refractive index of studied thin films were determined by the fitting procedure that combined the Wemple-DiDomenico's dispersion model[37] with Swanepoel's method for thin films on finite a substrate.[38] The transparent region of thin films' transmission spectra (extinction coefficient $k \rightarrow 0$) was fitted by Swanepoel's model of transmission spectrum (absorption in the thin films is neglected – *i.e.* $k = 0$), where the spectral dependence of the refractive index was expressed using the Wemple-DiDomenico's equation. This approach is particularly suitable for thin dielectric films where the transmission spectra exhibit too few interference fringes for the conventional Swanepoel method. The method's limitation is the necessary specular optical quality of analyzed thin films. The optical bandgap $E_g^{opt}$ was determined using Tauc's method for semiconductors.[39] Thickness, refractive index and optical bandgap values were obtained from 4 separate samples, averaged, and reported with standard deviation as error bars.

The atomic force microscopy (AFM) technique was employed to examine the surface topography and roughness of prepared samples. The thin films annealed at 180, 210, and 240 °C, as well as prepared diffraction gratings and EBL patterns, were analyzed by Solver NTEGRA (NT-MDT) microscope operating in semicontact (tapping) mode with NSG10 tips (AppNano). The measurements were conducted on 3 different 5 × 5 μm areas per sample. The surface roughness of studied thin films was evaluated from AFM scans as a root mean square (RMS) value, in accordance with the ISO 4287/1 norm. The depth of diffraction gratings and EBL patterns was derived from measured AFM scans. Reported error bars reflect the standard deviation of the measured values.

The structure of source bulk glasses, together with as-prepared and hard-baked samples, was studied by Raman spectroscopy. The analysis was performed by MultiRAM (Bruker) FT Raman spectrometer using a 1064 nm Nd:YAG laser excitation beam (2 cm$^{-1}$ resolution, 64 scans). The presented Raman spectra were normalized by the intensity of the most intense band in each individual spectrum.

A continuous-wave (cw) laser with 532 nm wavelength, Cobolt Samba 100 (Cobolt), was used to assess the photosensitivity of the studied samples. The $Ge_{25-x}In_xSe_{75}$ thin films hard-baked at 210 °C were exposed to a 50 mW laser beam for 10 min in an ambient atmosphere. The same device was also utilized for holographic recording using the interference-fringe field pattern generated by intersecting 532 nm laser beams (10 mW) with exposure times ranging from 10 to 60 seconds.

The wet etching technique was employed to determine the chemical resistance of both unexposed and exposed spin-coated $Ge_{25-x}In_xSe_{75}$ thin films hard-baked at 210 °C, as well as to develop latent images recorded by EBL and holography. Samples were etched in 1 vol% ethylenediamine (EDA) solution in dimethyl sulfoxide (DMSO) at 30 °C. The samples were submersed in the etching solution, and transmission spectra were continuously recorded *in situ* using a fiber-optic modular spectrometer BW-VIS (StellarNet). The samples with recorded latent images were etched for 25% of the total thin film's etching time to study processes induced by EBL and holography recording.

## Results and discussion

The differential scanning calorimetry (DSC) technique was used for the investigation of $Ge_{25-x}In_xSe_{75}$ ($x$ = 0, 2.5, 5, 7.5 and 10) bulk glasses, and their $T_g$ (Fig. 1) was determined from obtained DSC curves (Fig. S1–S5). It provides a valuable foundation for determining the suitable hard-baking temperatures of corresponding solution-processed thin films. Previously published results confirmed that the hard-baking of as-prepared solution-processed ChG thin films leads to material with a similar structure as the source bulk glass,[30,40,41] making the DSC data valid even for solution-processed thin films. The $Ge_{25}Se_{75}$ bulk glass possesses the highest $T_g$ (244 °C), which

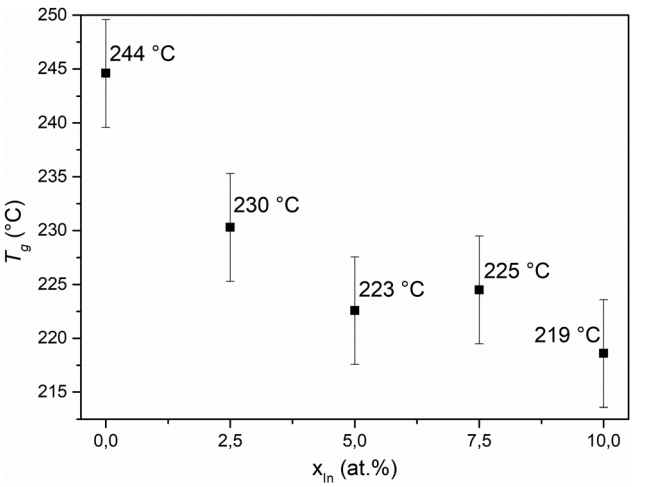


Fig. 1 The glass transition temperatures ($T_g$) of $Ge_{25-x}In_xSe_{75}$ ($x$ = 0, 2.5, 5, 7.5, and 10) bulk glasses obtained from DSC curves. The estimate error is 5 °C.

then steeply decreases with increasing indium content down to 219 °C for $Ge_{15}In_{10}Se_{75}$ bulk glass. Similarly to Ge–Sb–S or Ge–Sb–Se glasses,[33] the introduction of $In_2Se_3$ trigonal pyramidal units into a predominantly $GeSe_2$ tetrahedral matrix leads to an elevated structural disorder, resulting in a decrease of $T_g$.

The Ge–In–Se thin films were spin-coated from PA-MetOH solutions of source bulk glasses. The as-prepared films were hard-baked within 90–240 °C range to study the annealing-induced processes during thermal stabilization and identify the appropriate hard-baking temperature. The upper temperature limit (240 °C) was selected based on the $T_g$ of source bulk glasses, with $Ge_{25}Se_{75}$ films slightly exceeding this temperature while indium-containing ones were at or just below it. The energy-dispersive X-ray spectroscopy (EDX) technique was employed to verify the elemental composition of deposited thin films and to study the progress of the hard-baking process (Fig. 2). The representative EDX spectra are provided in Fig. S6. The results proved that the composition of as-prepared thin films was close to the targeted one. For the $Ge_{25}Se_{75}$ thin films, it remained stable through the whole hard-baking region. Contrary, the indium-containing thin films showed partial selenium loss, especially at 240 °C (up to 4% for $Ge_{15}In_{10}Se_{75}$ thin films). Observed partial chalcogen loss is consistent with previously published data,[33,42] and in our case, it was exacerbated by annealing above the $T_g$ of the corresponding bulk glass.

The content of amine and methanol organic residuals, occluded or bonded inside the glass matrix, was determined by the content of nitrogen and oxygen (Fig. 3a and b). The results indicate that the studied $Ge_{25-x}In_xSe_{75}$ as-prepared thin films contain a comparable amount of nitrogen-based residuals, but the content of methanol-based residuals significantly differs. The $Ge_{25}Se_{75}$ and $Ge_{22.5}In_{2.5}Se_{75}$ as-prepared thin films exhibit an oxygen content ranging from 9.1 to 9.5 at%, whereas $Ge_{17.5}In_{7.5}Se_{75}$ and $Ge_{15}In_{10}Se_{75}$ as-prepared thin films contain 5.9 at% of oxygen. As the hard-baking temperature rises, the organic residuals are gradually released, and the differences between the samples are highlighted. The organic residuals in $Ge_{25}Se_{75}$ thin films could be almost completely removed at 240 °C, although the as-prepared thin film contains the most methanol-based residuals. As the indium content rises, the thin films show a greater resistance to thermally induced release of both amine and methanol-based organic residuals. Although they cannot be removed completely, their content can still be significantly reduced. Due to the observed chalcogen loss, the hard-baking temperature at 210 °C provides a compromise between both competing processes and thus they were used for the patterning experiments.

The spin-coated $Ge_{25-x}In_xSe_{75}$ ($x$ = 0, 2.5, 5, 7.5, and 10) thin films were deposited in specular optical quality, and their thickness, along with their optical properties were determined from transmission spectra by the described evaluation procedure. Fig. S7–S11 show examples of fitted transmission spectra and optical bandgap evaluation using Tauc's method for samples hard-baked at 210 °C. The thermal dependence of thickness, refractive index, and optical bandgap are provided in Fig. 4 and Fig. S12 while the numerical values for as-prepared samples and samples hard-baked at 210 °C are provided in Table 1. The as-prepared thin films exhibit a gradual decrease in thickness with increasing indium content, despite using the identical solution concentration and spin-coating conditions. As the hard baking temperature rises, the treated thin films get gradually thinner due to the observed loss of organic residuals and the expected structural polymerization of the glass matrix. However, there is a noticeably higher thickness contraction for $Ge_{25}Se_{75}$ and $Ge_{22.5}In_{2.5}Se_{75}$ thin films (Fig. S12). It can be explained by the results from EDX analysis, which shows that as-prepared thin films of both compositions contain more methanol-based organic residuals that are simultaneously more readily removed at elevated temperatures.

The refractive index also increases with rising hard-baking temperature (Fig. 4a). The glass structure becomes more polymerized, dense and compact, with a lower content of amine or methanol-based residues. The hard-baked $Ge_{25}Se_{75}$ thin films exhibit the highest refractive index, while the indium-containing thin films are very similar to each other. Conversely, the optical bandgap of as-prepared thin films is significantly affected by the indium content, but upon the hard-baking, the values converge once again (Fig. 4b). Compared to $Ge_{25}Se_{75}$ thin films, the indium presence shifts short-wavelength absorption edge towards shorter wavelengths (blueshift). However, the optical bandgap is expected to decrease with increasing indium content.[29,43] The similarities in refractive index and optical bandgaps of indium-containing spin-coated thin films can probably be attributed to the EDX results discussed earlier. As the indium content rises, the residual content of organics in hard-baked thin films rises as well. The presence of low-index organic material then contributes to the refractive index of the Ge–In–Se thin film, influencing its total value. Consequently, in comparison with thermally evaporated $Ge_{20}In_5Se_{75}$ thin films,[44] the solution-processed counterparts exhibit a lower refractive index ($n_{1550}$ 2.20 *vs.* 2.36) and higher optical

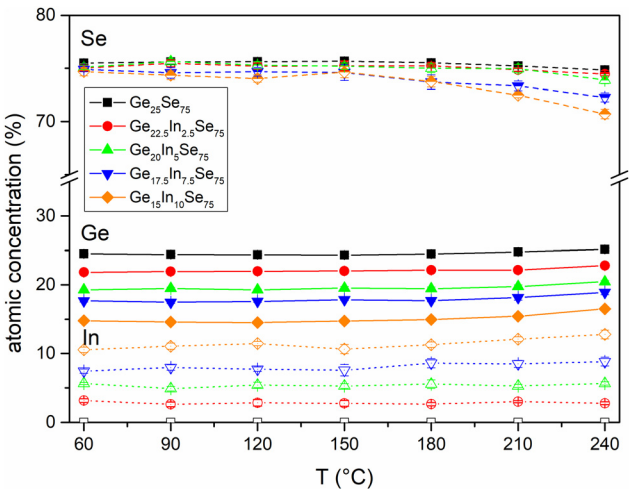


Fig. 2 The elemental composition of prepared $Ge_{25-x}In_xSe_{75}$ ($x$ = 0, 2.5, 5, 7.5, and 10) thin films as Ge : In : Se ratio (excluding the light elements) in dependence on hard-baking temperature.

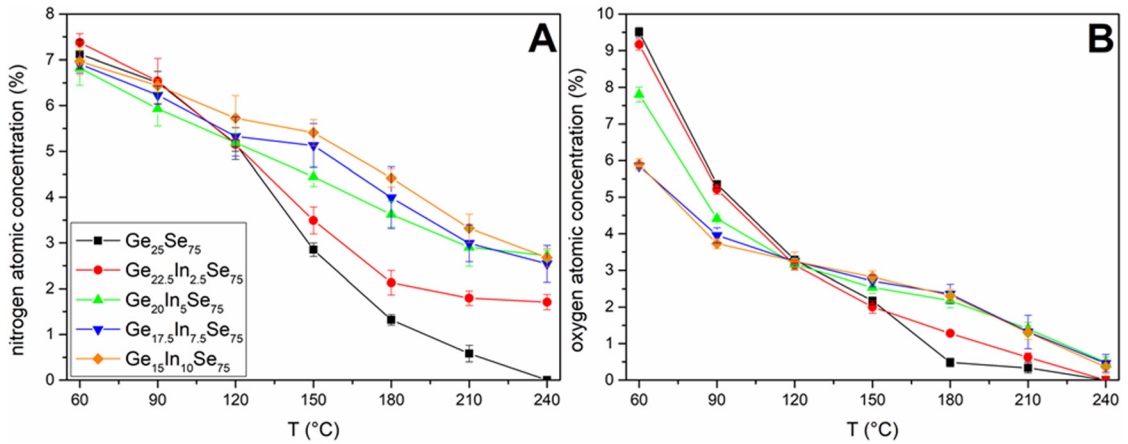


Fig. 3 The total nitrogen (A) and oxygen (B) content (as obtained from EDX analysis) in $Ge_{25-x}In_xSe_{75}$ ($x$ = 0, 2.5, 5, 7.5 and 10) thin films representing organic residuals in dependence on hard-baking temperature.

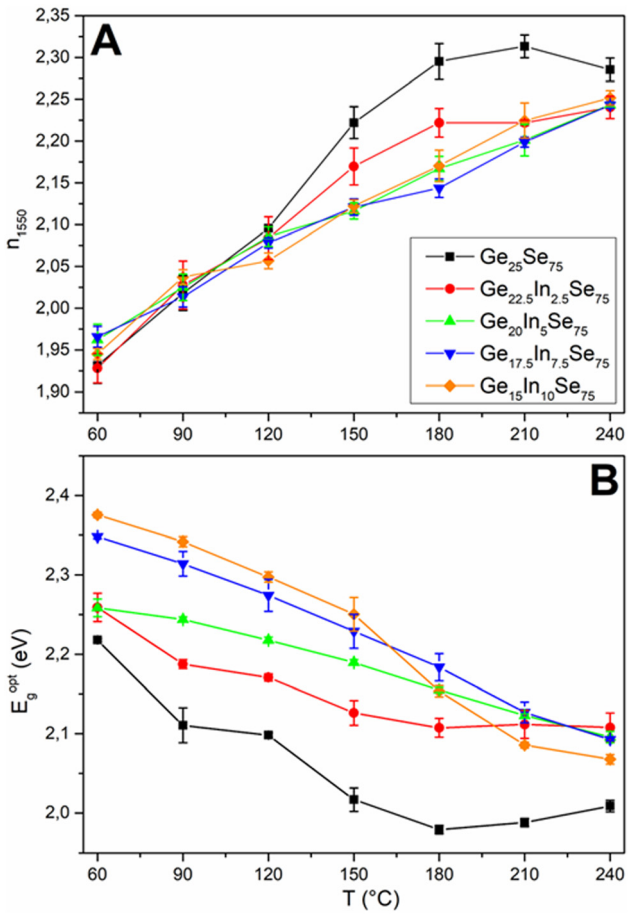


Fig. 4 The refractive index at 1550 nm $n_{1550}$ (A) optical bandgap $E_g^{opt}$ (B) of $Ge_{25-x}In_xSe_{75}$ ($x$ = 0, 2.5, 5, 7.5 and 10) thin films in dependence on hard-baking temperature.

Table 1 The thickness, refractive index at 1550 nm ($n_{1550}$), and optical bandgap ($E_g^{opt}$) of $Ge_{25-x}In_xSe_{75}$ ($x$ = 0, 2.5, 5, 7.5 and 10) thin films hard-baked at 210 °C. The thickness, refractive index and optical bandgap were determined from transmission spectra

| 60 °C | Thickness (nm) | $n_{1550}$ | $E_g^{opt}$ (eV) |
|---|---|---|---|
| $Ge_{25}Se_{75}$ | 360.2 ± 8.9 | 1.93 ± 0.02 | 2.22 ± 0.01 |
| $Ge_{22.5}In_{2.5}Se_{75}$ | 345.4 ± 14.3 | 1.93 ± 0.02 | 2.26 ± 0.02 |
| $Ge_{20}In_5Se_{75}$ | 298.2 ± 1.4 | 1.96 ± 0.02 | 2.26 ± 0.01 |
| $Ge_{17.5}In_{7.5}Se_{75}$ | 266.8 ± 5.8 | 1.97 ± 0.01 | 2.35 ± 0.01 |
| $Ge_{15}In_{10}Se_{75}$ | 280.3 ± 6.7 | 1.95 ± 0.01 | 2.38 ± 0.01 |
| 210 °C | Thickness (nm) | $n_{1550}$ | $E_g^{opt}$ (eV) |
| $Ge_{25}Se_{75}$ | 199.0 ± 5.4 | 2.31 ± 0.01 | 1.99 ± 0.01 |
| $Ge_{22.5}In_{2.5}Se_{75}$ | 214.3 ± 7.6 | 2.22 ± 0.01 | 2.11 ± 0.02 |
| $Ge_{20}In_5Se_{75}$ | 197.3 ± 3.4 | 2.20 ± 0.02 | 2.12 ± 0.01 |
| $Ge_{17.5}In_{7.5}Se_{75}$ | 181.6 ± 7.2 | 2.20 ± 0.01 | 2.13 ± 0.01 |
| $Ge_{15}In_{10}Se_{75}$ | 178.6 ± 8.8 | 2.22 ± 0.02 | 2.09 ± 0.01 |

Table 2 The RMS surface roughness of thin films annealed at 180, 210 and 240 °C derived from atomic force microscopy data

| RMS surface roughness (nm) | | | |
|---|---|---|---|
| | 180 °C | 210 °C | 240 °C |
| $Ge_{25}Se_{75}$ | 4.6 ± 0.1 | 1.3 ± 0.1 | 0.9 ± 0.4 |
| $Ge_{22.5}In_{2.5}Se_{75}$ | 2.4 ± 0.2 | 2.3 ± 0.1 | 2.3 ± 0.3 |
| $Ge_{20}In_5Se_{75}$ | 0.8 ± 0.2 | 0.9 ± 0.4 | 1.1 ± 0.1 |
| $Ge_{17.5}In_{7.5}Se_{75}$ | 0.9 ± 0.1 | 0.7 ± 0.1 | 2.1 ± 0.4 |
| $Ge_{15}In_{10}Se_{75}$ | 0.7 ± 0.1 | 0.6 ± 0.1 | 0.6 ± 0.2 |

bandgap ($E_g^{opt}$ 2.12 eV *vs.* 1.76 eV). The slight variations in refractive index and optical bandgap data (as indicated by the standard deviation) stem from the inherent limitations of the spin-coating technique. Although four separate samples were analyzed for each treatment, the manual nature of the spin-coating process introduces minor inconsistencies between samples.

The surface roughness defined by RMS and topography of thin films hard-baked at 180, 210 and 240 °C was studied by atomic force microscopy (AFM). The values of surface roughness are summarized in Table 2, and representative AFM scans are provided in Fig. 5 and Fig. S13–S17. The overall surface roughness remained very low (below 4.6 nm), contributing to the films' good optical quality. The AFM scans revealed

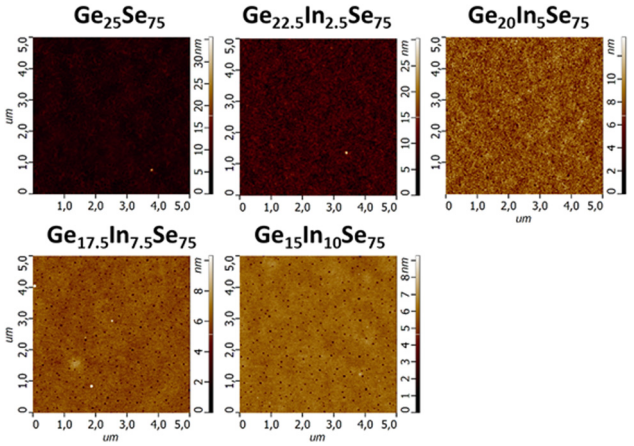


Fig. 5 The AFM scans of $Ge_{25-x}In_xSe_{75}$ ($x$ = 0, 2.5, 5, 7.5 and 10) thin films annealed at 210 °C.

the presence of small pores, particularly in the $Ge_{17.5}In_{7.5}Se_{75}$, and $Ge_{15}In_{10}Se_{75}$ thin films. Solution-processed chalcogenide glass thin films frequently exhibit pore formation, which has also been observed in other germanium-based samples.[32,33] The surface and cross-section of samples hard-baked at 210 °C was analyzed by SEM as well (Fig. S18). The SEM scans confirmed relatively smooth surface of deposited thin films, while the cross-sectional images showed no signs of extensive porosity. Nevertheless, the presence of a chalcogen-depleted thin surface layer is still expected.[33]

The Raman spectroscopy was employed to analyze the hard-baking induced structural changes in the studied $Ge_{25-x}In_xSe_{75}$ thin films. The Raman spectra of source bulk glasses (Fig. 6) confirmed the presence of dominant $GeSe_4$ corner- and edge-shared tetrahedrons with bands at 199 and 216 $cm^{-1}$.[45–47] The strong bands at 261 $cm^{-1}$ reveal the presence of distorted selenium rings attributed to selenium overstoichiometry.[45,46,48,49] The intensity of the band at 261 $cm^{-1}$ rises with increasing indium content.

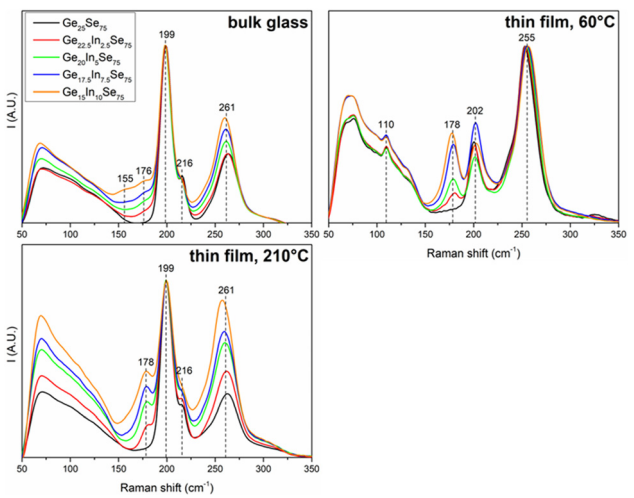


Fig. 6 The Raman spectra of $Ge_{25-x}In_xSe_{75}$ ($x$ = 0, 2.5, 5, 7.5, and 10) source bulk glasses together with the spectra of as-prepared thin films (60 °C) and thin films annealed at 210 °C.

The indium preferentially forms selenium-poorer $In_2Se_3$ pyramidal units rather than selenium-rich tetrahedra (as in the case of $GeSe_2$),[24] thereby contributing to the overall selenium overstoichiometry. The presence of $In_2Se_3$ pyramidal units is evidenced by the bands observed at 176 $cm^{-1}$, whose intensity increases with rising indium content.[43,50,51] Alternatively, the same Raman band might correspond to the [$Se_3Ge$–$GeSe_3$] vibrations,[52] however, due to the substantial selenium overstoichiometry, their presence is unlikely. In the case of $Ge_{15}In_{10}Se_{75}$ bulk glass, the additional weak band at 155 $cm^{-1}$ can be distinguished in the measured Raman spectrum. It can be attributed to the vibrations of [$InSe_4$] tetrahedrons,[43,53,54] whose formation is likely associated with the availability of non-bonded selenium. As confirmed by EXAFS analysis,[55] the mean coordination number of indium in selenium-rich ChGs varies between 3.3-3.5, suggesting that while the majority of indium atoms have three neighbours, some indium atoms are tetrahedrally coordinated by Se.

As already discussed, the hard-baked solution-processed thin films usually possess a structure close to the source bulk glasses. However, the structure of as-prepared thin films is usually very different due to the generally fragmented glass network and the presence of organic residues, both as non-bonded (occluded) organic molecules and chemically bonded amines in the form of alkyl ammonium salts.[30,32] The dominant band at 255 $cm^{-1}$ can be attributed to the vibrations of selenium with a distorted ring network structure, potentially influenced by organic residuals. The weak band at 110 $cm^{-1}$ can also be associated with vibrations of distorted selenium rings. It should be noted that the bands at 178 $cm^{-1}$, associated with $In_2Se_3$ units, are already well developed, indicating that these structural units are likely not bonded to amine residues as salts, but instead exist as free units within the unpolymerized structure of the as-prepared thin films. As the hard-baking temperature increased, the dominant Raman bands of selenium with a distorted ring structure gradually diminished while the Raman bands of $GeSe_4$ corner- and edge-shared (199 and 216 $cm^{-1}$) tetrahedrons intensified. Thus, the hard-baking of as-prepared thin films leads to more compact and polymerized material. While selenium loss was detected (particularly in In-rich compositions), the deficiency remains relatively low – approx. 2.2 at% for $Ge_{15}In_{10}Se_{75}$ thin films annealed at 210 °C. Hard-baked films retain a high chalcogen overstoichiometry as reflected in the strong intensity of the selenium band. Although the structure of thin films hard-baked at 210 °C more closely resembles that of the corresponding bulk glasses, notable differences remain (especially for indium-rich samples). The bands corresponding to the vibrations of $In_2Se_3$ pyramidal units are more pronounced, vibrations of [$InSe_4$] tetrahedrons are entirely absent, and the bands of selenium with a distorted ring structure exhibit increased intensity. We assume that the $In_2Se_3$ units are significantly harder to incorporate back into the polymerized glass network, and excess selenium tends to form distorted rings rather than acting as a bridging element or contributing to [$InSe_4$] tetrahedra.

The photosensitivity of Ge–In–Se solution-processed thin films annealed at 210 °C was investigated using a cw 532 nm

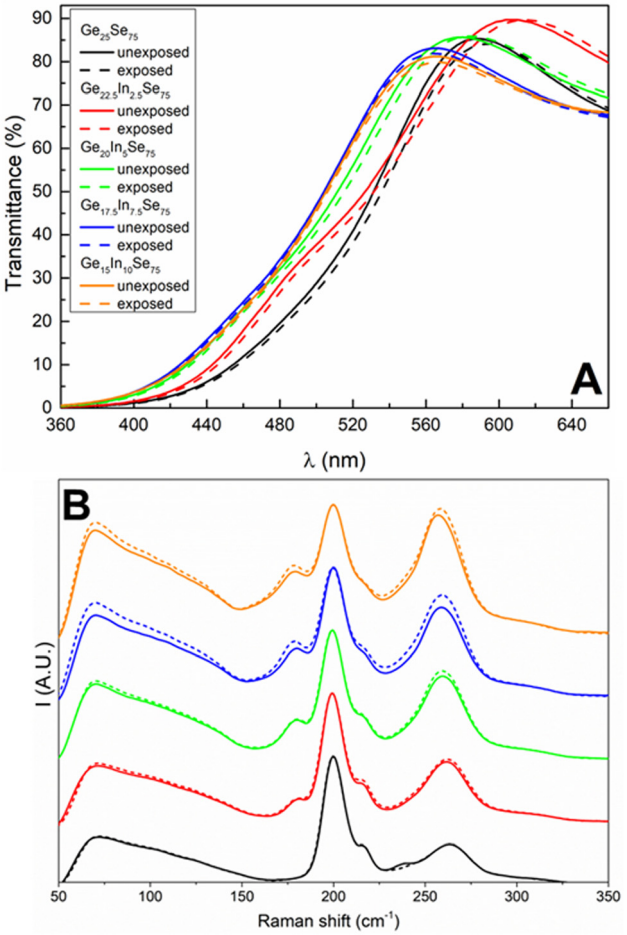


Fig. 7 The transmission (A) and Raman spectra (B) of $Ge_{25-x}In_xSe_{75}$ ($x$ = 0, 2.5, 5, 7.5 and 10) thin films annealed at 210 °C before (solid line) and after 532 nm exposure (dashed line).

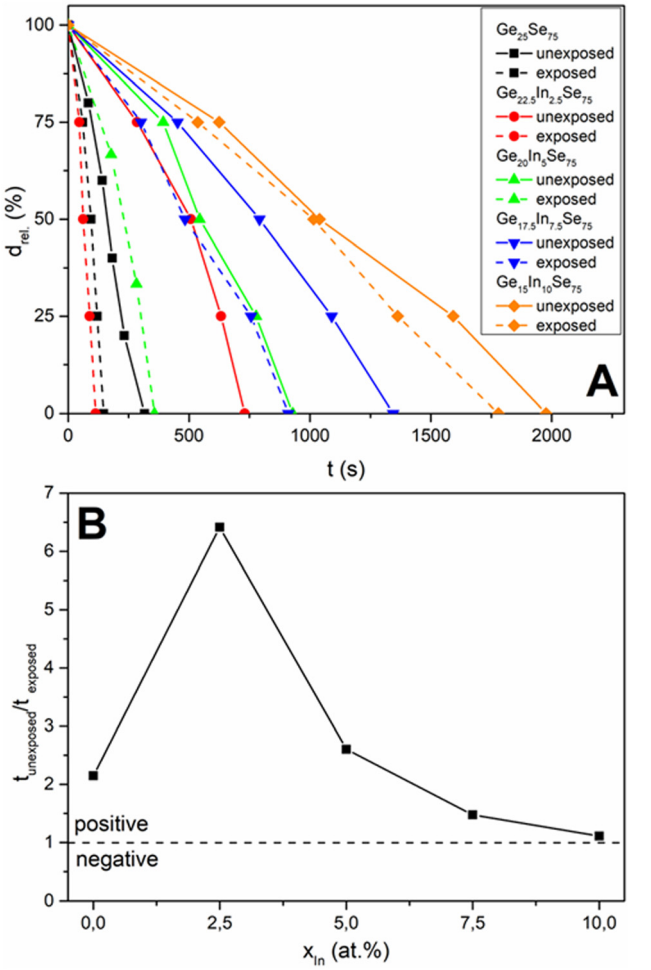


Fig. 8 The etching curves (A) and etching rates ratios (B) of $Ge_{25-x}In_xSe_{75}$ ($x$ = 0, 2.5, 5, 7.5 and 10) thin films annealed at 210 °C before and after 532 nm exposure.

laser beam exposure (50 mW, 10 min). Hard-baking at 210 °C significantly reduces the content of organic residuals while maintaining the composition close to the targeted one. The UV-Vis transmission spectra revealed the minor exposure-induced red shift of the short-wavelength absorption edge (Fig. 7), suggesting a photo-darkening response. The Raman spectra exhibited only slight variations, mainly in the increased intensities of the bands corresponding to distorted selenium rings and $In_2Se_3$ pyramidal units.

Although the structural and optical changes of the studied Ge–In–Se thin films are relatively minor, exposure-induced changes in chemical resistance were found to be more pronounced (Fig. 8). Both unexposed and exposed thin films were etched in 1% EDA–DMSO solution. The derived etching curves (Fig. 8a) and etching rate ratios (Fig. 8b) demonstrated positive etching selectivity, characteristic of spin-coated chalcogenide glass thin films.[41,56,57] The data showed that the incorporation of a small amount of indium (2.5 at%) dramatically enhances the photosensitivity of the studied thin films, but a further increase in indium content results in the reduction of photosensitivity. Moreover, the $Ge_{17.5}In_{7.5}Se_{75}$ and $Ge_{15}In_{10}Se_{75}$ thin films possess even lower photosensitivity than indium-free $Ge_{25}Se_{75}$ thin films. In contrast, the $Ge_{22.5}In_{2.5}Se_{75}$ thin films demonstrate one of the highest etching selectivity (6.4) ever reported for solution-processed chalcogenide thin films (*e.g.* 1.8 for $As_{30}S_{70}$,[56] 3.9 for $As_{20}Ge_{12.5}S_{67.5}$,[57] or 2.4 for $Ge_{20}Sb_5S_{75}$[41]).

The exposure-induced changes in etching rates were exploited for the fabrication of diffraction gratings using a holographic recording technique. The $Ge_{25-x}In_xSe_{75}$ thin films hard-baked at 210 °C were exposed to the interference-fringe field of 532 nm laser beam (10 mW) for 10–60 seconds. Exposed samples were subsequently developed in 1% EDA–DMSO solvent for 25% of the unexposed thin film's etching time. The depths of the obtained sinusoidal diffraction gratings were determined using AFM, and summarised data are presented in Fig. 9. The representative AFM scans of holographic diffraction gratings prepared by 50 s exposure are provided in Fig. S19. The graph proves that $Ge_{22.5}In_{2.5}Se_{75}$ thin films possess the highest photosensitivity, followed by $Ge_{25}Se_{75}$, $Ge_{20}In_5Se_{75}$, and $Ge_{17.5}In_{7.5}Se_{75}$ thin films. The sinusoidal minima of the diffraction grating formed in the $Ge_{22.5}In_{2.5}Se_{75}$ thin film after 60 s of

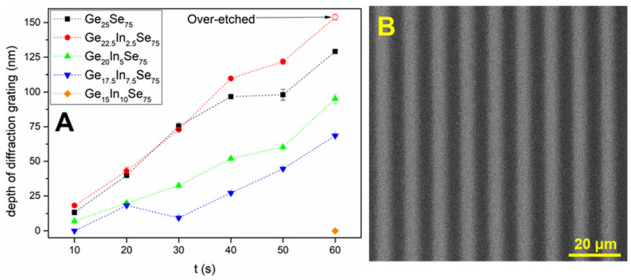


Fig. 9 The depths of diffraction gratings fabricated in $Ge_{25-x}In_xSe_{75}$ ($x$ = 0, 2.5, 5, 7.5 and 10) thin films annealed at 210 °C (A) along with the SEM scan of a representative diffraction grating (B). No diffraction gratings were produced in $Ge_{15}In_{10}Se_{75}$ thin films.

exposure were etched completely through the film, reaching the substrate (indicating over-etching). No diffraction gratings were prepared in $Ge_{15}In_{10}Se_{75}$ thin films due to the poor etching selectivity of exposed material and low resolution of the interference fringe field pattern.

The photosensitive chalcogenides often possess sensitivity to electron beam exposure as well.[41,58] Thus, the electron beam lithography (EBL) technique was employed to investigate the sensitivity of studied spin-coated thin films to electrons. The set of EBL patterns was recorded (50–1250 μC cm$^{-2}$ dose), wet-etched in 1% EDA–DMSO solvent (developing for 25% of the unexposed thin film's etching time), and analyzed by AFM (Fig. 10). The SEM scans (Fig. 11) confirmed that the exposed regions were etched faster than the unexposed ones, mirroring the behaviour observed in laser-exposed thin films. However, electron sensitivity exhibits a different trend, with $Ge_{22.5}In_{2.5}Se_{75}$ thin films showing the highest sensitivity, followed by $Ge_{20}In_5Se_{75}$ and $Ge_{17.5}In_{7.5}Se_{75}$ thin films with approximately equal sensitivity, while $Ge_{25}Se_{75}$ and $Ge_{15}In_{10}Se_{75}$ thin films show the lowest sensitivity. Therefore, the indium incorporation enhances the electron sensitivity of solution-processed $Ge_{25-x}In_xSe_{75}$ thin films up to 7.5% indium content. The SEM scans of etched material in Fig. 11 also revealed that the exposed material exhibits greater surface roughness than the surrounding unexposed areas, while this effect diminishes with increasing indium content.

Presented results show that the Ge–In–Se solution-processed thin films exhibit promising properties which could outweigh

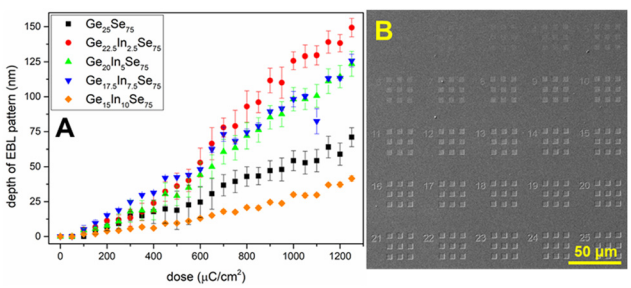


Fig. 10 The depths of EBL patterned $Ge_{25-x}In_xSe_{75}$ ($x$ = 0, 2.5, 5, 7.5, and 10) thin films annealed at 210 °C in dependence on electron exposure dose (A) together with the SEM scan of a typical EBL pattern (B).

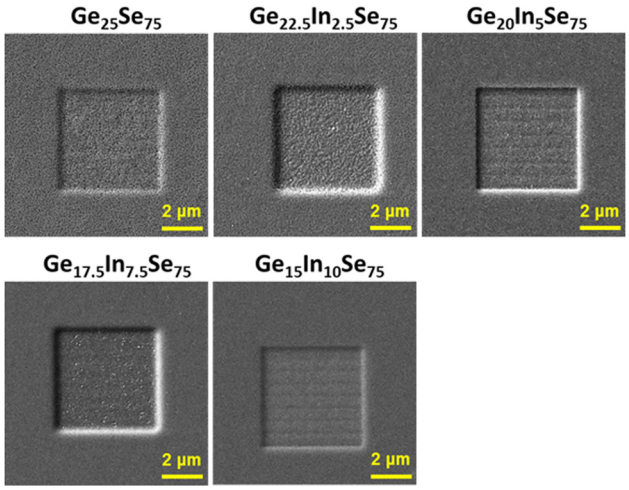


Fig. 11 The SEM scans of EBL patterned $Ge_{25-x}In_xSe_{75}$ ($x$ = 0, 2.5, 5, 7.5, and 10) thin films annealed at 210 °C exposed with a 750 μC cm$^{-2}$ dose.

shortcomings stemming from the presence of organic residuals and enable their widespread application on an industrial scale. The absence of toxic elements, high refractive index, excellent chemical stability, the possibility for surface patterning by holographic or electron beam lithography techniques and good etching selectivity (especially for $Ge_{22.5}In_{2.5}Se_{75}$) highlight their suitability for potential practical applications.

## Conclusions

The DSC was used to determine the $T_g$ of the $Ge_{25-x}In_xSe_{75}$ ($x$ = 0, 2.5, 5, 7.5, and 10) source bulk glasses, which decreased with increasing indium content (from 244 °C for $Ge_{25}Se_{75}$ to 219 °C for $Ge_{15}In_{10}Se_{75}$). The DSC data also guided the selection of hard-baking temperatures for the solution-processed thin films within the 60–240 °C region. The Ge–In–Se thin films were prepared in specular optical quality *via* spin-coating. The EDX confirmed that as the indium content increased, the thin films exhibited a gradual tendency for thermally-induced selenium loss, especially at 240 °C (up to 4% for $Ge_{15}In_{10}Se_{75}$ thin films), while this effect was exacerbated by annealing above the $T_g$ of the corresponding bulk glass. Similarly, the thin films showed a greater resistance for thermally induced release of both amine and methanol-based organic residuals with increasing indium content.

With increasing hard-baking temperature, the removal of organic residuals and associated structural changes resulted in decreased thin film thickness and optical bandgap, alongside an increase in refractive index. At 240 °C, the optical parameters of the indium-containing samples gradually converged, probably due to the varying content of low-index organic material, which subsequently contributed to the refractive index and optical bandgap of Ge–In–Se thin films. The AFM scans of hard-baked samples revealed low surface roughness and the presence of small pores, particularly in the $Ge_{17.5}In_{7.5}Se_{75}$ and $Ge_{15}In_{10}Se_{75}$ thin films. The Raman spectroscopy confirmed the

expected thermally-induced structural polymerization, leading to the materials with a structure close to the source bulk glasses. However, $In_2Se_3$ units proved harder to incorporate back into the polymerized glass network.

The photo- and electron-sensitivity of hard-baked $Ge_{25-x}In_xSe_{75}$ thin films were investigated using a 532 nm laser beam exposure and electron beam lithography technique, while the recorded latent images were developed by subsequent wet-etching. Both experiments demonstrated that the initial addition of 2.5 at% indium significantly enhanced electron and photo-sensitivity, whereas further increases in indium content resulted in a decline in these properties. Moreover, the $Ge_{22.5}In_{2.5}Se_{75}$ thin films showed one of the highest etching selectivity (6.4) ever reported for solution-processed thin films.

## Author contributions

J. Ja. and A. M.: investigation; formal analysis; methodology, visualization, S. S.: conceptualization; writing; investigation; formal analysis; data curation; supervision, M. K.: investigation; formal analysis, R. S.: investigation; formal analysis, J. Je.: investigation; formal analysis, M. V and K. P.: supervision; resources; methodology; funding acquisition.

## Conflicts of interest

There are no conflicts to declare.

## Data availability

Data for this article are available in the Figshare repository at **https://doi.org/10.6084/m9.figshare.29253089**.

DSC curves; EDX spectra of as-prepared and annealed thin films; fitted transmission spectra and optical bandgap evaluation using Tauc's method; thin film thickness and thickness contraction; AFM scans of thin films and holographic gratings; and cross-sectional SEM images. See DOI: **https://doi.org/10.1039/d5ma00596e**

## Acknowledgements

The authors appreciate the financial support from grant LM2023037 from the Ministry of Education, Youth and Sports of the Czech Republic and OISE-2106457 project from NSF Ires1 program.

## References

1 A. V. Kolobov and K. Shimakawa, World Scientific Reference of Amorphous Materials, Structure, Properties, Modeling and Main Applications, 2020.
2 J.-L. Adam and X. Zhang, Chalcogenide Glasses: Preparation, Properties and Applications, 2014.
3 D. H. Cha, Y. Hwang, J.-H. Kim, D.-S. Kim and H.-J. Kim, *Proc. SPIE*, 2014, **9249**, 924916.
4 A. Zoubnir, M. Richardson, C. Rivero, A. Schulte, C. Lopez, K. Richardson, M. Ho and R. Vallee, *Opt. Lett.*, 2004, **29**, 748–750.
5 G. Lucovsky and J. Philips, *J. Non-Cryst. Solids*, 2008, **19–25**, 2753–2756.
6 W. Blanc, Y. G. Choi, X. Zhang, M. Nalin, K. Richardson, G. C. Righini, M. Ferrari, A. Jha, J. Massera, S. Jiang, J. Ballato and L. Petit, *Prog. Mater. Sci.*, 2023, **134**, 101084.
7 A. S. Hassanien, I. Sharma and A. K. Aly, *Phys. B*, 2021, **613**, 412985.
8 Y. Saito, M. Morota, K. Makino, K. Tominaga, A. V. Kolobov and P. Fons, *Mater. Sci. Semicond. Process.*, 2021, **135**, 106079.
9 X. Wu, F. Lai, L. Lin, J. Lv, B. Zhuang, Q. Yan and Z. Huang, *Appl. Surf. Sci.*, 2008, **254**, 6455–6460.
10 Y. Zha, M. Waldmann and C. B. Arnold, *Opt. Mater. Express*, 2013, **3**, 1259–1272.
11 R. A. Tabrizi, A. Rezvani and A. Rasooli, *Opt. Mater.*, 2023, **136**, 113431.
12 R. Gadhwal, H. Singh, A. Devi and K. Kumar, *Opt. Laser Technol.*, 2023, **157**, 108665.
13 N. S. Dutta and C. B. Arnold, *Trends Chem.*, 2021, **3**, 535–546.
14 K. Palka, T. Syrovy, S. Schroter, S. Bruckner, M. Rothhardt and M. Vlcek, *Opt. Mater. Express*, 2014, **4**, 384–395.
15 S. Novak, P. T. Lin, C. Li, C. Lumdee, J. Hu, A. Agrawal, P. G. Kik, W. Deng and K. Richardson, *Appl. Mater. Interfaces*, 2017, **9**, 26990–26995.
16 S. Novak, D. E. Johnston, C. Li, W. Deng and K. Richardson, *Thin Solid Films*, 2015, **588**, 56–60.
17 S. Tzadka, N. Ostrovsky, E. Toledo, D. Le Saux, E. Kassis, S. Joseph and M. Schvartzman, *Opt. Express*, 2020, **28**, 28352–28365.
18 M. Kurka, K. Palka, J. Jancalek, S. Slang and M. Vlcek, *J. Non-Cryst. Solids*, 2021, **559**, 120674.
19 S. Novak, L. Scarpantonio, K. Novak, M. D. Pre, A. Martucci, J. D. Musgraves, N. D. McClenaghan and K. Richardson, *Opt. Mater. Express*, 2013, **3**, 729–738.
20 H. Khan, P. K. Dwivedi, M. Husain and M. Zulfequar, *J. Mater. Sci.: Mater. Electron.*, 2018, **29**, 12993–13004.
21 M. V. Kovalenko, R. D. Schaller, D. Jerzab, M. A. Loi and D. V. Talapin, *J. Am. Chem. Soc.*, 2012, **134**, 2457–2460.
22 Z. U. Borisova, *Glassy Semiconductors*, 1981.
23 G. Saffarini, *Phys. B*, 1998, **253**, 52–55.
24 J. Ledru, J. M. Saiter, G. Saffarini and S. Benazeth, *J. Non-Cryst. Solids*, 1998, **232–234**, 634–637.
25 A. Giridhar and S. Mahadevan, *J. Non-Cryst. Solids*, 1992, **151**, 245–252.
26 S. S. Fouad, M. S. El-Bana, P. Sharma and V. Sharma, *Appl. Phys. A:Mater. Sci. Process.*, 2015, **120**, 137–143.
27 S. Muhavedan and A. Giridhar, *J. Mater. Sci.*, 1994, **29**, 3837–3842.
28 G. Mathew and J. Philip, *J. Phys.: Condens. Matter*, 1999, **11**, 5283.
29 N. H. Teleb, W. A. Abd El-Ghany and A. M. Salem, *J. Non-Cryst. Solids*, 2021, **572**, 121103.
30 S. Slang, P. Janicek, K. Palka and M. Vlcek, *Opt. Mater. Express*, 2016, **6**, 1973–1985.

31 S. M. R. Ullah, A. A. Simon and M. Mitkova, *Microsc. Microanal.*, 2019, **25**, 2608–2609.
32 M. Waldman, J. D. Musgraves, K. Richardson and C. B. Arnold, *J. Mater. Chem.*, 2012, **22**, 17848–17852.
33 S. Slang, M. Kurka, J. Jancalek, J. Rodriguez-Pereira, M. Chylii, J. Houdek, J. Jemelka, R. Svoboda, J. Bartak, M. Vlcek and K. Palka, *Appl. Surf. Sci.*, 2024, **672**, 160744.
34 D. B. Mitzi, *Adv. Mater.*, 2009, **21**, 3141–3158.
35 R. Zhang, S. Cho, D. G. Lim, X. Hu, E. A. Stach, C. A. Handwerker and R. Agrawal, *Chem. Commun.*, 2016, **52**, 5007–5010.
36 H. Khan, P. K. Dwivedi, S. Islam, M. Husain and M. Zulfequar, *Opt. Mater.*, 2021, **119**, 111332.
37 S. H. Wemple and M. DiDomenico, *Phys. Rev. B*, 1973, **3**, 1338.
38 R. Swanepoel, *J. Phys. E: Sci. Instrum.*, 1983, **16**, 1214.
39 J. Tauc, *Mater. Res. Bull.*, 1970, **5**, 721–729.
40 S. Slang, K. Palka, J. Jancalek, M. Kurka and M. Vlcek, *Opt. Mater. Express*, 2020, **10**, 2973–2986.
41 S. Slang, P. Janicek, K. Palka, L. Loghina and M. Vlcek, *Mater. Chem. Phys.*, 2018, **203**, 310–318.
42 J. Jemelka, K. Palka, P. Janicek, S. Slang, J. Jancalek, M. Kurka and M. Vlcek, *Sci. Rep.*, 2023, **13**, 16609.
43 R. Todorov, E. Cernoskova, P. Knotek, Z. Cernosek and M. Vlasova, *J. Non-Cryst. Solids*, 2018, **498**, 415–421.
44 H. E. Atyia, *Phys. B*, 2008, **403**, 16–24.
45 R. Holomb, V. Mitsa, E. Akalin, S. Akyuz and M. Sichta, *J. Non-Cryst. Solids*, 2013, **373–374**, 51–56.
46 R. K. Pan, H. Z. Tao, H. C. Zang, X. J. Zhao and T. J. Zhang, *J. Alloys Compd.*, 2009, **484**, 645–648.
47 C. Jiang, X. Wang, Q. Zhu, Q. Nie, M. Zhu, P. Zhang, S. Dai, X. Shen, T. Xu, C. Cheng, F. Liao, Z. Liu and X. Zhang, *Infrared Phys. Technol.*, 2015, **73**, 54–61.
48 A. H. Goldan, C. Li, S. J. Pennycook, J. Schneider, A. Blom and W. Zhao, *J. Appl. Phys.*, 2016, **120**, 135101.
49 K. Nagata, T. Ishikawa and Y. Miyamoto, *Jpn. J. Appl. Phys.*, 1985, **24**, 1171–1173.
50 K. D. Machado, M. C. Siqueira, D. Jastrombek, C. A. Duarte, S. M. de Souza, E. A. Cotta and S. F. Stolf, *Eur. Phys. J. B*, 2013, **86**, 90.
51 J. Weszka, P. Daniel, A. Burian, A. M. Burian and A. T. Nguyen, *J. Non-Cryst. Solids*, 2000, **265**, 98–104.
52 G. Tang, C. Liu, Z. Yang, L. Luo and W. Chen, *J. Non-Cryst. Solids*, 2009, **355**, 1585–1589.
53 H. Xiong, G. Tang, L. Luo and W. Chen, *Jpn. J. Appl. Phys.*, 2011, **50**, 102602.
54 Y. Xu, H. Zeng, G. Yang, G. Chen, Q. Zhang and L. Xu, *Opt. Mater.*, 2008, **31**, 75–78.
55 I. Kaban, P. Jovari, T. Petkova, P. Petkov, A. Stoilova, W. Hoyer and B. Beuneu, *J. Phys.: Condens. Matter*, 2010, **22**, 404205.
56 S. Slang, K. Palka, H. Jain and M. Vlcek, *J. Non-Cryst. Solids*, 2017, **457**, 135–140.
57 S. Slang, K. Palka and M. Vlcek, *J. Non-Cryst. Solids*, 2017, **471**, 415–420.
58 P. Janicek, S. Funke, P. H. Thiesen, S. Slang, K. Palka, J. Mistrik, M. Grinco and M. Vlcek, *Thin Solid Films*, 2018, **660**, 759–765.